

# Do eddies connect the tropical Atlantic Ocean and the Gulf of Mexico?

F. Andrade-Canto

Departamento de Observación y  
Estudio de la Tierra, la Atmósfera y  
el Océano

El Colegio de la Frontera Sur  
Chetumal, Quintana Roo, Mexico  
fernando.andrade@ecosur.mx

F.J. Beron-Vera

Department of Atmospheric Sciences  
Rosenstiel School of Marine &  
Atmospheric Science  
University of Miami  
Miami, Florida, USA  
fberon@miami.edu

Started: February 3, 2022. This version: September 23, 2022.

## Abstract

Consistent with satellite-tracked trajectories of drogued drifters, but at odds with Eulerian assessment of satellite-altimetry measurements of sea-surface height, we show that North Brazil Currents Rings (NBCRs) are incapable of bypassing the Lesser Antilles as structures that coherently transport material. The nature of the inability of the de-facto oceanographic Eulerian, streamline-based eddy detection technique to produce a correct assessment is rooted in its lack of objectivity. We arrive at this conclusion by applying *geodesic eddy detection* on the altimetric dataset over nearly its entire extent. While we detect northwestward translating NBCRs that can be classified as coherent Lagrangian eddies, they typically experience strong filamentation and complete loss of coherence prior to reaching the Lesser Antilles. Moreover, the filamented material hardly penetrates into the Caribbean Sea, let alone the Gulf of Mexico, and not without substantively mixing with the ambient fluid east of the archipelago.

## Plain Language Summary

Geodesic eddy detection is a Lagrangian (fluid-parcel-following) method that objectively, i.e., in an observer-independent manner, reveals eddies (fluid regions spinning about a common axis) with material (fluid) boundaries that defy the exponential stretching that arbitrary material loops typically experience in turbulent flow. Eddies instantaneously revealed as regions enclosed by streamlines in general do not have such a property: the topology of the streamlines depends on the observer viewpoint. Thus instantaneously closed streamlines cannot be guaranteed to hold and carry within material. Here we use geodesic eddy detection to demonstrate that North Brazil Current rings detected from their Eulerian footprints in the altimetric sea-surface height field do not connect the tropical Atlantic Ocean and the Gulf of Mexico.

## Key Points

- The topology of SSH streamlines is observer dependent and hence are eddies from the AVISO+ META database
- Geodesic eddy detection objectively reveals eddies with stretching resisting material boundaries that also minimize diffusion
- North Brazil Current Ring contents hardly penetrate into the Caribbean without mixing with the ambient fluid east of the Lesser Antilles

## 1 Introduction

Huang et al. [2021] have recently argued that eddies, more specifically mesoscale anticyclonic North Brazil Current Rings (NBCRs), connect the tropical Atlantic Ocean and the Gulf of Mexico. NBCRs are offsprings of the North Brazil Current retroflection [Johns et al., 1990; Didden and Schott, 1993; Goni and Johns, 2001; Wilson et al., 2002; Johns et al., 2003; Goni and Johns, 2003; Garraffo et al., 2003]. As mesoscale oceanic eddies, they have potential long-range ability of dragging along various types of tracers (e.g., nutrients, salinity, larvae) [Robinson, 1983], and, in particular, *Sargassum* rafts [Beron-Vera and Miron, 2020]. The argument of Huang et al. [2021] is based on the tracking of Eulerian *footprints* of mesoscale vortices on satellite-altimetry gridded maps of sea-surface height (SSH) anomaly [Schlax and Chelton, 2016] and absolute dynamic topography [Rio et al., 2011]. Here we refute this claim and support our rebuttal on observations by Fratantoni and Richardson [2004] of satellite-tracked surface drifters and submerged floats, which show that they hardly traverse the Lesser Antilles. The main issue with the flawed analysis by Huang et al. [2021] is the observer-dependent nature of their analysis. We reiterate below, one more time, the issue with the Eulerian, streamline-based analysis carried out by Huang et al. [2021], no matter how sophisticated it is made (e.g., through lagged correlations and the construction of Hovmöller plots of stitched fields on one side and of the other of the Lesser Antilles) or how arbitrary it is framed (e.g., by following a particular isoline of SSH).

Consider the velocity field  $\mathbf{u}(\mathbf{x}, t) = (x \sin 4t + y(2 + \cos 4t), x(\cos 4t - 2) - y \sin 4t)$ , where  $\mathbf{x} = (x, y) \in \mathbb{R}^2$  denotes position and  $t \in \mathbb{R}$  is time, which represents an exact linear solution of the two-dimensional Navier–Stokes equation [Haller, 2005]. The flow streamlines are closed at all times suggesting an elliptic structure, i.e., a vortex. Moreover, the most common Eulerian criteria ( $Q$ ,  $\lambda_2$ ,  $\Delta$ , swirling strength, etc., cf. Haller [2005]) invariably suggest that the flow holds a vortex. In particular, the de-facto oceanographic eddy detection diagnostic [Chelton et al., 2011], following a simple-minded argument by Flierl [1981], classifies the flow as a “nonlinear vortex” since  $U/c = \infty$ , where  $U$  is the rotational speed around the vortex and  $c$  is the (here vanishing) propagation speed of the vortex. However, if a tracer is initialized within one instantaneously closed streamline, the tracer does not remain trapped within the streamline as time goes by, but rather it stretches bypassing all instantaneously closed streamlines (Fig. 1, middle panels).

The behavior just described has an explanation: this flow actually hides a rotating saddle (pure deformation), as it follows by making  $\mathbf{x} \mapsto \bar{\mathbf{x}}(\mathbf{x}, t) = (x \cos 2t - y \sin 2t, x \sin 2t + y \cos 2t)$ , under which  $\mathbf{u}(\mathbf{x}, t) \mapsto (\bar{y}, \bar{x}) \equiv \bar{\mathbf{u}}(\bar{\mathbf{x}})$ . The  $\bar{\mathbf{x}}$ -frame is special inasmuch the flow in

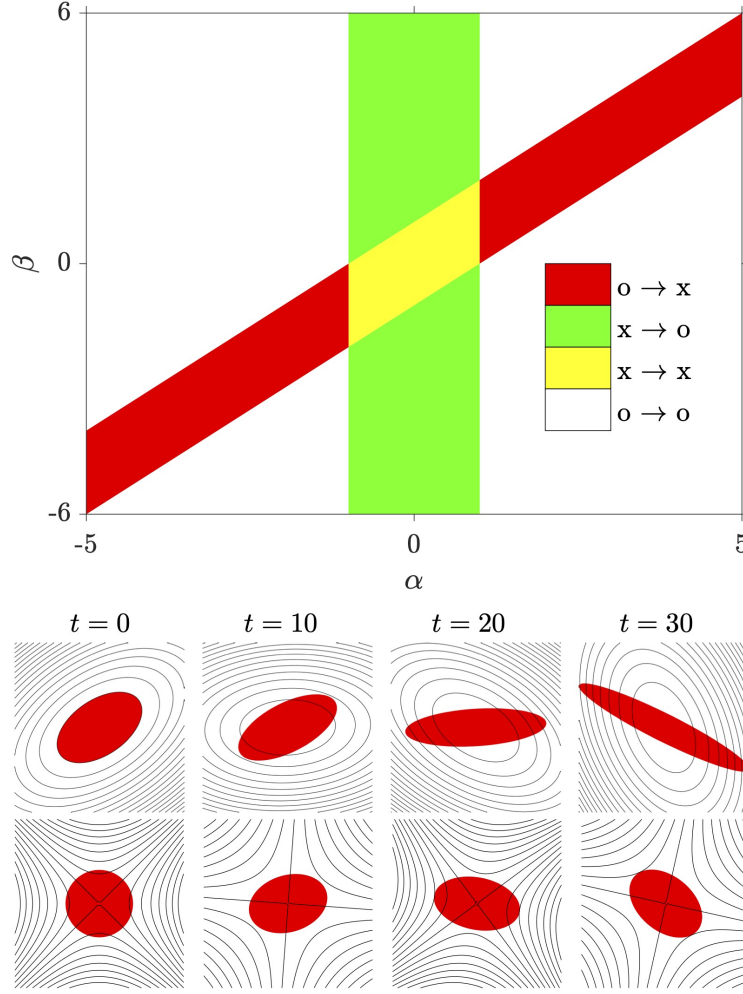


Figure 1: (top panel) For the velocity field  $\mathbf{u}(\mathbf{x}, t) = (x \sin 2\beta t + y(\alpha + \cos 2\beta t), x(\cos 2\beta t - \alpha) - y \sin 2\beta t)$ , exact solution of the Navier-Stokes equation in two-space dimensions, complete possible streamline topology transformations under the observer change  $\mathbf{x} \mapsto \bar{\mathbf{x}}(\mathbf{x}, t) = (x \cos \beta t - y \sin \beta t, x \sin \beta t + y \cos \beta t)$ , where “o” refers to center and “x” to saddle. (middle panels) Snapshots the evolution of a passive tracer (red) initially within a closed streamline of the velocity field with  $(\alpha, \beta) = (2, 2)$ . (bottom panels) As in the middle panels, but with  $(\alpha, \beta) = (0, 4)$

this frame is steady, and thus flow streamlines and fluid trajectories coincide. Hence short-term exposition pictures of the velocity field by the observer in the  $\bar{\mathbf{x}}$ -frame determine the long-term fate of fluid particles. The only additional observation to have in mind to fully determine the Lagrangian motion is that the observer in the  $\bar{\mathbf{x}}$ -frame rotates (at angular speed 2). This tells us that the flow under consideration is not actually unsteady as there is a frame (the  $\bar{\mathbf{x}}$ -frame) in which it is steady.

The situation can be made even more dramatic if the more general linear solution to the two-dimensional Navier-Stokes equation is considered:  $\mathbf{u}(\mathbf{x}, t) = (x \sin 2\beta t + y(\alpha +$

$\cos 2\beta t), x(\cos 2\beta t - \alpha) - y \sin 2\beta t)$  where  $\alpha, \beta \in \mathbb{R}$  are arbitrary constants. For instance, for  $(\alpha, \beta) = (0, 4)$  one observes in the  $\beta$ -spinning  $\mathbf{x}$ -frame a fixed saddle, while when viewed in the rotating frame  $\mathbf{x} \mapsto \bar{\mathbf{x}}(\mathbf{x}, t) = (x \cos \beta t - y \sin \beta t, x \sin \beta t + y \cos \beta t) = (x \cos 8t - y \sin 8t, x \sin 8t + y \cos 8t)$ , one observes a center, meaning that a seemingly purely deforming flow actually is a pure rotation flow structure! That is, a material vortex. This is illustrated in the bottom panels of Fig. 1. The complete possible streamline topology transformations in parameter space are presented in top panel of Fig. 1, where “o” refers to center (pure rotation) and “x” to saddle (pure deformation). If the exact solution so far discussed is considered “pathological” for being linear, [Pedergrana et al. \[2020\]](#) discuss a *nonlinear* solution which exhibits behavior similar to that just described.

In a truly unsteady flow there is no such distinguished observer for whom the flow is steady [[Lugt, 1979](#)]. Thus one can never be sure which observer gives the right answer when Eulerian vortex detection—particularly the de-facto oceanographic vortex detection diagnostic [[Chelton et al., 2011](#)—is applied. As a consequence, neither false positives nor false negatives can be ruled out [[Beron-Vera et al., 2013](#)], and thus life expectancy estimates drawn from such diagnostics are unreliable [[Andrade-Canto et al., 2020](#)].

In this Letter we show the results of applying a Lagrangian, observer-independent eddy detection technique, known as *geodesic eddy detection* [[Haller and Beron-Vera, 2013, 2014](#)], on the altimetry record over 1995-2019. This, of course, goes way beyond observing closed streamlines of the altimetric SSH field [[Chelton et al., 2011](#)]. We reveal a number of NBCRs with material boundaries capable of dragging material along. However, no NBCR is found to bypass the Lesser Antilles as a coherent material structure. The NBCRs have relatively short-lived coherent material cores, experiencing strong breakaway filamentation before reaching the Lesser Antilles, consistent with the drifter and float observations by [Fratantoni and Richardson \[2004\]](#).

## 2 Methodology

### 2.1 Geodesic Eddy Detection

Let  $\mathbf{u}(\mathbf{x}, t)$  be a two-dimensional fluid velocity, with  $\mathbf{x}$  denoting position in some domain of  $\mathbb{R}^2$  and  $t \in \mathbb{R}$  referring to time. Let  $\mathbf{F}_{t_0}^t(\mathbf{x}_0)$  denote the solution of fluid particle motion equation

$$\dot{\mathbf{x}} = \mathbf{u}(\mathbf{x}, t) \quad (1)$$

for initial condition  $\mathbf{x}(t_0) = \mathbf{x}_0$ . Note that  $\mathbf{F}_{t_0}^t$  relates time- $t_0$  and  $t$  positions of fluid particles, and thus is called a  $(t_0, t)$ -flow map.

The notion of a vortex with a material boundary resisting stretching under advection by the flow, e.g., as inferred geostrophically from altimetry data, from time  $t_0$  to time  $t_0 + T$  for some (finite)  $T$  is expressed by the variational principle [[Haller and Beron-Vera, 2013, 2014](#)]:

$$S[\mathbf{r}] := \oint \frac{\sqrt{\langle \mathbf{r}'(s), \mathbf{C}_{t_0}^{t_0+T}(\mathbf{r}(s)) \mathbf{r}'(s) \rangle}}{\sqrt{\langle \mathbf{r}'(s), \mathbf{r}'(s) \rangle}} ds = 0, \quad \left. \frac{d}{d\epsilon} \right|_{\epsilon=0} S[\mathbf{r} + \epsilon \mathbf{n}] = 0. \quad (2)$$

Here,  $\mathbf{r}(s)$  provides a parametrization for a material loop at time  $t_0$ ,  $\mathbf{n}(s)$  is normal to the curve,

$$\mathbf{C}_{t_0}^{t_0+T}(\mathbf{x}_0) := D\mathbf{F}_{t_0}^{t_0+T}(\mathbf{x}_0)^\top D\mathbf{F}_{t_0}^t(\mathbf{x}_0) \quad (3)$$

is the (coefficient of the symmetric, positive-definite, right) *Cauchy–Green strain tensor field*, and the angle bracket denotes scalar product. The integrand in (2), which objectively (i.e., independent of the observer’s viewpoint) measures relative stretching from  $t_0$  to  $t_0 + T$ , is invariant under  $s$ -shifts and thus represents a Noether quantity. That is, it is equal to a positive constant, say  $p$ . In other words, solutions to (2) are characterized by uniformly  $p$ -stretching loops. Embedded within  $O(\varepsilon)$ -thick coherent material belts showing no observable variability in averaged relative stretching, the time- $t_0$  positions of such  $p$ -loops turn out to be limit cycles of one of the following two bidirectional vector or *line* fields:

$$\mathbf{l}_p^\pm(\mathbf{r}) := \sqrt{\frac{\lambda_2(\mathbf{r}) - p^2}{\lambda_2(\mathbf{r}) - \lambda_1(\mathbf{r})}} \mathbf{v}_1(\mathbf{r}) \pm \sqrt{\frac{p^2 - \lambda_1(\mathbf{r})}{\lambda_2(\mathbf{r}) - \lambda_1(\mathbf{r})}} \mathbf{v}_2(\mathbf{r}), \quad (4)$$

where  $\lambda_1 < p^2 < \lambda_2$ . Here,  $\{\lambda_i\}$  and  $\{\mathbf{v}_i\}$ , satisfying  $0 < \lambda_1 \leq \lambda_2$ ,  $\langle \mathbf{v}_i, \mathbf{v}_j \rangle = \delta_{ij}$ ,  $i, j = 1, 2$ , are eigenvalues and (orientationless) normalized eigenvectors, respectively, of  $\mathbf{C}_{t_0}^{t_0+T}(\mathbf{x}_0)$ . Limit cycles of (4) either grow or shrink under changes in  $p$ , forming smooth annular regions of nonintersecting loops. The outermost member of such a band of material loops is observed physically as the boundary of a *coherent Lagrangian eddy*. The  $p$ -loops can also be interpreted as so-called null-geodesics of the (sign-indefinite) *generalized Green–Lagrangian tensor field*,  $\mathbf{C}_{t_0}^{t_0+T}(\mathbf{x}_0) - p \text{Id}$  [Haller and Beron-Vera, 2014]. For this and related results [Haller and Beron-Vera, 2012; Beron-Vera et al., 2013; Haller, 2015] we refer to this method of vortex identification as *geodesic eddy detection*.

Material loops characterized by  $p = 1$  resist the universally observed material stretching in turbulence: they reassume their initial perimeter at time  $t_0 + T$ . This conservation of perimeter, along with the conservation of the enclosed area in the incompressible case, conveys extraordinary coherence to geodesically detected eddies.

An important observation is that the boundaries of coherent material vortices revealed from geodesic detection are not only stretching resisting, but also are nearly diffusion resisting [Haller et al., 2018]. This may be expected for material fluid lines that do not experience folding, and it is reassuring that it can be formally proved.

## 2.2 Numerical Implementation

Clearly, making reliable assessments of eddy material transport requires one to pay a computational price. Geodesic eddy detection is now well-documented [Haller and Beron-Vera, 2013, 2014; Karrasch et al., 2014; Karrasch and Schilling, 2020] and software tools are available. We call the attention of the reader to the **Julia** implementation employed here, **CoherentStructures.jl**. Nevertheless, we consider instructive to briefly summarize the algorithmic steps involved in geodesic eddy detection, enabling the practitioner to implement them in his/her preferred programming language:

1. Provide  $\mathbf{u}(\mathbf{x}, t)$  with  $(\mathbf{x}, t) \in (\mathcal{D}, \mathcal{I}) \subset \mathbb{R}^2 \times \mathbb{R}$  and fix  $t_0 \in \mathcal{I}$  and  $|T| < \text{length}(\mathcal{I})$ . Here we use  $\mathbf{u} = g f^{-1} \hat{\mathbf{z}} \times \nabla \eta$ , where  $g \hat{\mathbf{z}}$  is gravity,  $f$  is the Coriolis parameter, and  $\eta(\mathbf{x}, t)$  is

the altimetric SSH (i.e., with mean dynamic topography added), as provided by the Archiving, Validation and Interpretation of Satellite Oceanographic data (AVISO+).

2. Integrate  $\mathbf{u}$  over  $t \in [t_0, t_0 + T]$  for initial conditions  $\mathbf{x}_0$  on fine lattice  $\mathcal{G}$  covering  $\mathcal{D}$  well to get  $\mathbf{F}_{t_0}^{t_0+T}(\mathbf{x}_0)$  using some high-order method, such as the Runge–Kutta family.
3. Finite differentiate  $\mathbf{F}(\mathbf{x}_0)$  over  $\mathcal{G}$  to get  $\mathbf{C}_{t_0}^{t_0+T}(\mathbf{x}_0)$  and compute  $\mathbf{C}_{t_0}^{t_0+T}\xi = \lambda\xi$ .
4. Construct the  $p$ -line fields  $\mathbf{l}_p^\pm$ .
5. Using index theory for planar line fields [Karrasch et al., 2014], identify  $\mathcal{D}_s \subset \mathcal{D}$  with  $\text{ind}_{\partial\mathcal{D}_s}(\mathbf{l}_p^\pm) = 1$ , viz., with  $\mathbf{x}_0^*$  satisfying  $\mathbf{C}_{t_0}^{t_0+T}(\mathbf{x}_0^*) = \text{Id}$  such that the number of wedges ( $\text{ind} = \frac{1}{2}$ ) exceeds that of trisectors ( $\text{ind} = -\frac{1}{2}$ ) by 2 (wedges and trisectors are the only type of singular points, analogous to critical points of vector fields, in two-space dimensions). This is a necessary condition for the existence of a limit cycle of the  $p$ -line field [Karrasch et al., 2014].
6. Identify fixed points in Poincare sections transversal to  $\mathbf{l}_p^\pm$  in each  $\mathcal{D}_s$  and keep the outermost of all. Each corresponding limit cycle defines the boundary of a coherent material vortex that defies stretching over  $t \in [t_0, t_0 + T]$ .

A refined version of this algorithm, proposed in Andrade-Canto et al. [2020] and utilized here, exhaustively searches the two-dimensional parameter space  $(t_0, T)$ , *allowing to frame genesis and apocalypse*. More specifically, the refinement consists in repeatedly applying geodesic eddy detection on the (altimetric) flow domain of definition as follows:

7. Roll the initial time instance  $t_0$  over a time window covering the time interval of during which a vortex is expected to exist.
8. For each  $t_0$ , progress  $T$  as long as a coherent Lagrangian eddy is successfully detected. This way, for each  $t_0$  a life expectancy  $T_{\text{exp}}(t_0)$  is obtained, which is the maximum  $T$  for which a geodesic eddy over  $[t_0, t_0 + T]$  is successfully detected. The expected result is a wedge-shaped  $T_{\text{exp}}(t_0)$  distribution, indicating that all Lagrangian coherence assessments predict the breakdown consistently, independent of any parameter presets. The *birth date*,  $t_{\text{bday}}$ , of the vortex is given by the  $t_0$  for which  $T_{\text{exp}}(t_0)$  is maximized. The *decease date* is then  $t_{\text{bday}} + T_{\text{exp}}(t_{\text{bday}})$ .

Robust assessments of the birth and decease dates of the vortex may be obtained by combining the results from running the algorithm in forward- and backward-time directions.

### 3 Results

An important cautionary remark is in order regarding using currents derived geostrophically from altimetry in our analysis. Depending of how parameters are selected, the validity of the (quasi)geostrophic modeling framework may be brought as close to, or as far away from, the equator as desired. We here have chosen to stand middle ground between being too permissive and too stringent by setting the lower limit of the domain of analysis to

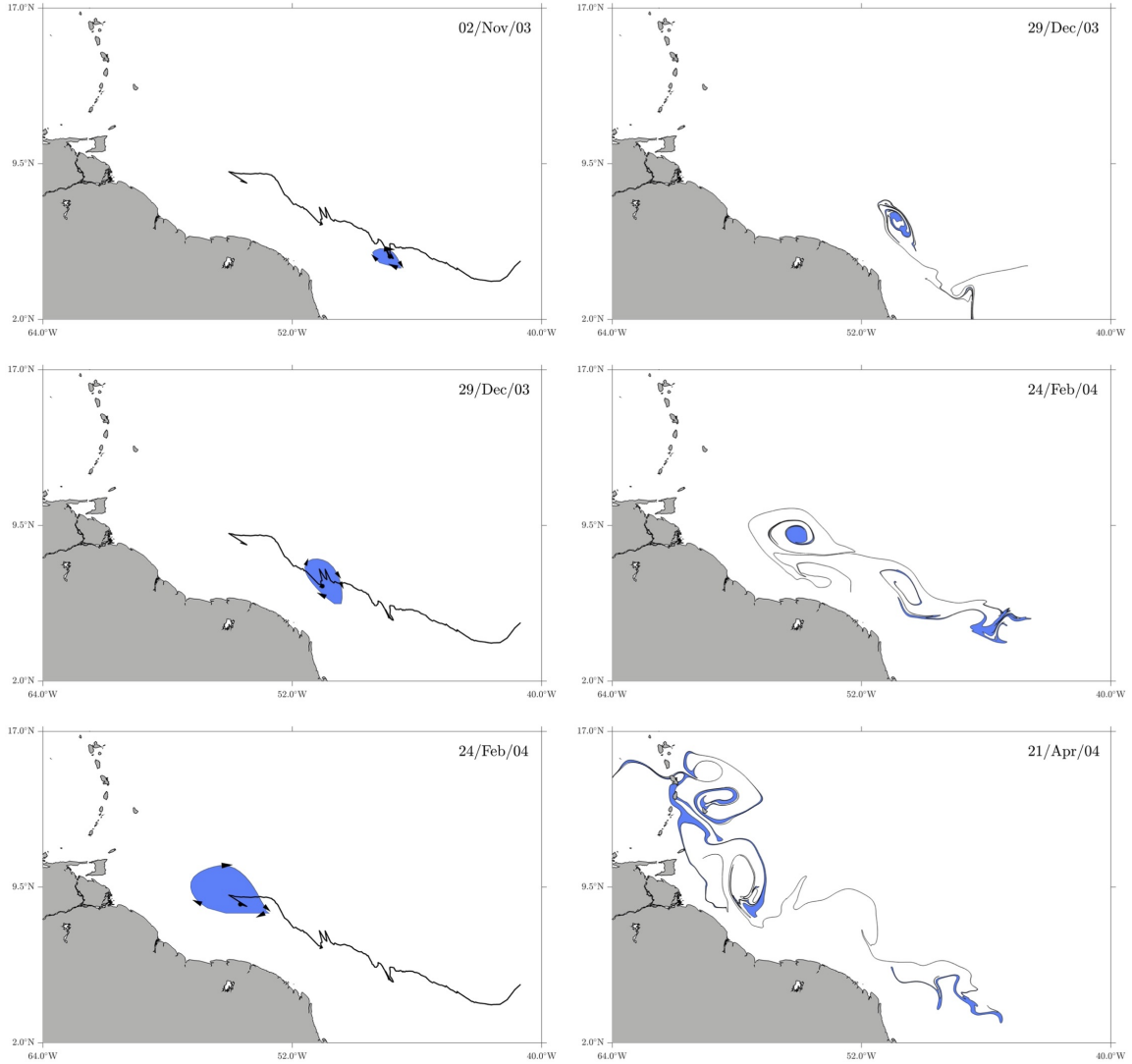


Figure 2: (left panels) Selected snapshots of an NBCR classified as a nonlinear SSH eddy by the AVISO+ META database over 13/Aug/03 through 24/Feb/04. The black curve in each panel corresponds to track #74667 from this dataset. The arrows indicate the instantaneous direction of the flow along the SSH streamline that defines the boundary of the eddy on each day shown. (right panels) Advected images after 57 days of each of the SSH eddy snapshots in the left panel under the altimetry-derived flow.

2°N. At this latitude the Rossby number is about 0.7, as one can infer it based on independent satellite drifter and float tracking estimates of NBCR typical diameters (249 km) and azimuthal velocities ( $90 \text{ cm s}^{-1}$ ) by [Fratantoni and Richardson \[2004\]](#).

Before applying geodesic eddy detection, we consider track #74667 the AVISO+ Mesoscale Eddy Trajectory Atlas Product (META) [\[Pegliasco et al., 2022\]](#) to show that the tracked SSH feature neither bypasses the Lesser Antilles as implied by [Huang et al. \[2021\]](#),



nor it coherently transports fluid. The former is evident from the naked-eye inspection of track #74667, which is shown in the left column of Fig. 2 along with 57-day-apart snapshots of the corresponding SSH eddy, taken to be the region bounded by the outermost closed SSH level set following Chelton et al. [2011]. Track #74667 never reaches the Lesser Antilles, and thus prolonging this trajectory into the Caribbean Sea as in Figs. 2a–b of Huang et al. [2021] is indefensible. Moreover, the instantaneous geostrophic velocity field rotates anticyclonically along track #74667, and the vector field shown by Huang et al. [2021] immediately west of the Lesser Antilles inside the eastern Caribbean rotates cyclonically! On the other hand, the nonlinear parameter for this SSH eddy  $10 < U/c < 25$  approximately from 13/Aug/03 through 24/Feb/04. However, it does not hold within and transport along fluid coherently as instructed by the de-facto oceanographic eddy detection method [Chelton et al., 2011]. This is demonstrated in the right column of Fig. 2, which shows forward advected images after 57 days of each SSH eddy snapshot in the left column under the altimetry-derived flow. Note the vigorous filamentation experienced by each SSH eddy snapshot upon advection. Clearly, the fluid mass initially inside the SSH eddy snapshot on 13/Aug/03 is not mapped into that of 29/Dec/03 and neither is the mass initially the latter into that on 24/Feb/04. The flow is (nearly) incompressible, so from the change of size of the SSH feature tracked is already quite obvious, without the need of advection whatsoever, that one is not in the presence of a coherent material vortex. However, there is evidence of material being trapped inside the “core” of the SSH eddy while tracked over 29/Dec/03–24/Feb/04. This suggests, and we confirm below, that its positions during this time period are intersecting those of a coherent Lagrangian vortex. The SSH eddy snapshot on 24/Feb/04 was forward-advected 57 days despite track #74667 ends on 24/Feb/04 to check if fluid initially inside traverses the Lesser Antilles. Some fluid is indeed seen to penetrate into the Caribbean Sea, consistent with direct measurements of biogeochemical tracers [Johns et al., 2014]. But this is accompanied by substantial filamentation, even southeastward, more consistent with the observed resistance of drifters and floats to bypass the Lesser Antilles Fratantoni and Richardson [2004] than with NBCRs connecting the tropical Atlantic with the Caribbean Sea [Huang et al., 2021].

We now proceed to applying geodesic eddy detection. Starting by taking SSH eddy track #74667 as a reference, we were able to extract an anticyclonic coherent Lagrangian vortex, identifiable with an NBCR. The vortex acquired material coherence on  $t_{\text{bday}} = 07/\text{Feb}/04$ , which lasted until 20/Mar/04. This corresponds to a rigorous material coherence life expectancy of  $T_{\text{exp}}(t_{\text{bday}}) = 42$  days, which maximizes the function  $T_{\text{exp}}(t_0)$  obtained by rolling the coherence assessment time,  $t_0$ , over the duration of SSH eddy track #74667, and progressing the integration time,  $T$ , until no vortex boundary is geodesically extracted. This explains why some material was seen to be trapped inside the SSH eddy corresponding to track #74667: the SSH eddy snapshot on 29/Dec/03 intersects the advected image on that date of the geodesically detected vortex on  $t_{\text{bday}} = 07/\text{Feb}/04$ . This vortex falls on the shorter side of the mesoscale spectrum, with an *equivalent radius*  $r_{\text{eq}} = 35$  km. We define  $r_{\text{eq}}$  as the average over the time interval  $[t_{\text{bday}}, t_{\text{bday}} + T_{\text{exp}}(t_{\text{bday}})]$  of the radii of the circumferences whose perimeters are equal to those of the forward-advected images over that interval of the boundary of the extracted coherent Lagrangian vortex on  $t_{\text{bday}}$ . The perimeter of the material boundary of the NBCR in question is further characterized by growing over its lifespan by a factor  $p = 2$ . This exemplifies well its characteristic property,



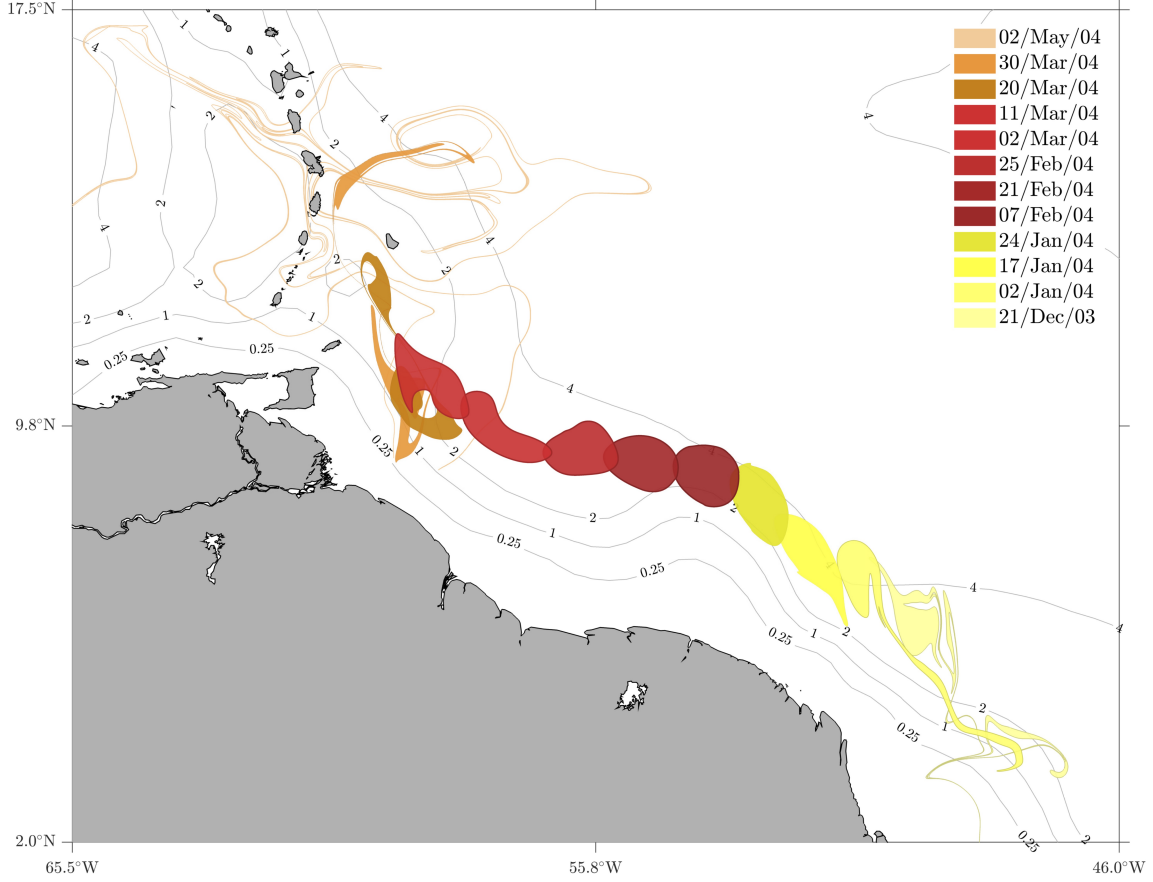


Figure 3: Genesis (yellow), evolution (red), and apocalypse (orange) of a coherent Lagrangian NBCR, geodesically detected from altimetry-derived velocity data using the SSH eddy trajectory of Fig. 2 as a reference. Selected isobaths (in km) are shown in gray.

namely, a strong tendency to resist stretching. In Fig. 6 we illustrate the life cycle of the geodesically detected NBCR, indicating in red tones the material vortex while is classified as coherent. In yellow tones we show several backward-time images of the NBCR on  $t_{\text{bday}} = 07/\text{Feb}/04$ , illustrating its genesis. This happens at around  $52^\circ\text{W}$ , consistent with assessments of NBCR formation from the analysis of satellite-derived chlorophyll images [Fratantoni and Glickson, 2002] and also of float and drifter trajectories [Fratantoni and Richardson, 2004]. How material coherence is acquired is a formidable problem, which admittedly lies beyond the reach of the nonlinear dynamics tool employed here. We note, however, that it must build on some underlying physical process. Priorly proposed “NBCR pinch off” mechanisms include potential vorticity transformation in the nonlinear cross-equatorial flow of the NBC [Edwards and Pedlosky, 1998; Zharkov and Nof, 2010] and barotropic instability of the North Equatorial Counter Current and ensuing radiation of Rossby waves [Jochum and Malanotte-Rizzoli, 2003]. Several forward-advected images of the NBCR on  $t_{\text{bday}} + T_{\text{exp}}(t_{\text{bday}}) = 20/\text{Mar}/04$  are depicted in orange tones. This illustrates the apocalypse of the NBCR, whose contents do not traverse the Lesser Antilles

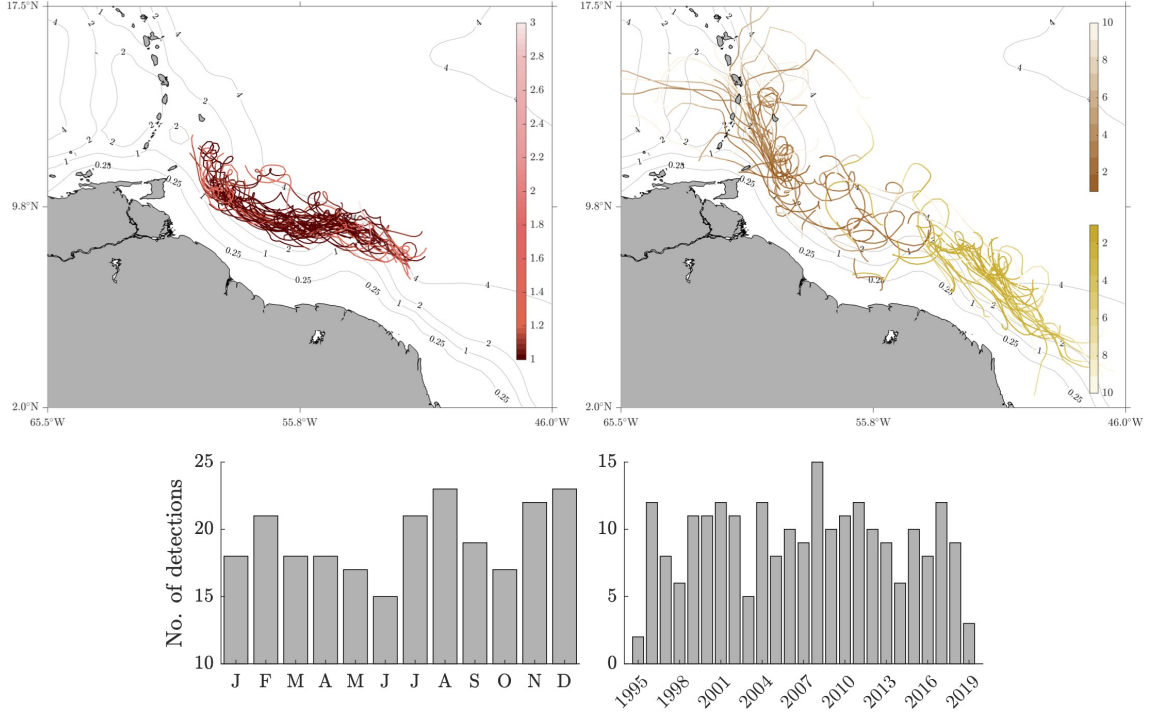


Figure 4: (top-left panel) Trajectories of the centroids of geodesically detected NBCRs over 1995–2019 from altimetry-derived velocity with colors indicating stretching factor ( $p$ ). (top-right panel) Thirty-day-backward (resp., forward) trajectories of the centroids of the regions occupied by the geodesically detected NBCRs on their birth (resp., decease) date. The backward (resp., forward) trajectories are depicted using yellowish (resp., brownish) colors, whose tonalities decrease with increasing relative stretching of the boundary of the advected fluid regions. (bottom-left) Number of coherent Lagrangian NBCRs detected as a function of the month. (bottom-right) As in the left, but as a function of the year.

coherently. Indeed, the NBCR loses material coherence several hundreds of km away from the Antilles Arc, when encountering water depths shallower than 2000 m, which applies to many other geodesically detected NBCRs as we show below. According to in-situ hydrography [Fratantoni et al., 1995], the anticyclonic circulation of NBCRs may be traced down in the water column as deep as 1000 m. This seems sufficiently deep for them to become unstable due to topographic effects. But surface-intensified NBCRs have also been observed [Wilson et al., 2002], suggesting that they may bypass topography without difficulty [Adams and Flierl, 2010] and thus other mechanisms, such as thermal instability as proposed by Andrade-Canto et al. [2022] for Caribbean Sea eddies, might be contributing to their loss of material coherence. This is a much more tractable problem than material coherence acquisition, and is reserved for near future investigation. (Subsurface NBCRs have also been identified [Johns et al., 2003], but these are not detectable from altimetry and thus are beyond the scope of this paper.)

Geodesic eddy detection is finally applied over a long period of time, 1995 through 2019. A census of coherent Lagrangian NBCRs is constructed, independent of reference

SSH eddy tracks. More specifically, we repeatedly search for coherent Lagrangian NBCRs by applying geodesic eddy detection inside a  $7^\circ \times 8^\circ$  box centered at  $(9^\circ\text{N}, 54^\circ\text{W})$ . While this is a region where NBCR shedding can be expected to take place [Fratantoni and Glickson, 2002; Fratantoni and Richardson, 2004], if a vortex is geodesically detected on some  $t_0$  for some *trial* integration time  $T$ , its centroid is advected in *backward* time until geodesic detection applied in *forward* time does not detect any vortex, enabling framing genesis with precision. Steps 7 and 8 of the geodesic eddy detection algorithm (Sec. 2.2) are then applied starting on the last  $t_0$  for which a vortex is detected. Rolling  $t_0$  forward from that  $t_0$  does not require any SSH eddy trajectory as a reference, as the trajectory of the centroid of the geodesically detected vortex is employed. In the top-left panel of Fig. 4 we show the trajectories of the centroids of all geodesically detected NBCRs. These are colored according to their stretching factor ( $p$ ). Out of a total of 196 NBCRs detected over 1995–2019, none was seen to reach the Lesser Antilles as a coherent material vortex. Rigorous material coherence is lost in many cases when a ring approaches the 1500-m isobath or so. On average, coherent material NBCRs possess a life time of  $T_{\text{exp}}(\text{bday}) = 30 \pm 18$  d, stretch by a factor of  $p = 1.2 \pm 0.35$ , and have an equivalent radius of  $r_{\text{eq}} = 42 \pm 16$  km. The bottom-left (resp., right) panel at the bottom of Fig. 4 shows the number of geodesically detected NBCRs as a function of the month (resp., year). While the number varies (from 2 to 15) along the year, no statistically significant seasonal (annual or annual-plus-semiannual) signal is seen to fit the observed variability. In turn,  $9 \pm 3$  coherent material NBCRs are formed yearly on average, revealing no statistically significant trend of any sign. Finally, in the top-right panel of Fig. 4 we show the trajectories of the centroids of the regions occupied by the backward (resp., forward) advected images of the initial (resp., final) positions of the boundaries of the geodesically detected NBCRs for 30 days. We use yellowish (resp., brownish) colors for the backward (resp., forward) trajectory pieces. The tonality of these colors decreases with increasing relative stretching of the advected boundaries, computed as the ratio of initial-to-final advected boundary arclength. Note, in particular, that relative stretching increases considerably near the Lesser Antilles, indicating that the contents of material NBCRs, once coherent, get mixed with the ambient fluid in the Atlantic before a typically small fraction thereof finds its way into the Caribbean Sea.

We have intentionally avoided entering the debate over the reliability of transport calculations based on altimetry-derived velocities, with diverging views, cf., e.g., Poje et al. [2017] as an example of a critical view and Beron-Vera and LaCasce [2016] with a contrasting opinion. However, in response to the request of an anonymous reviewer, we have included in the Supporting Information a figure (S1) which provides support for the latter, more positive view, with a comparison of a geodesic eddy detection based on velocities as provided by AVISO+ on the standard  $0.25^\circ \times 0.25^\circ$  grid and on velocities from the experimental Multiscale Interpolation Ocean Science Topography (MIOST), which are higher-resolution velocities on a  $0.1^\circ \times 0.1^\circ$  grid that combine AVISO+ velocities and velocities from available surface buoys from the NOAA Global Drifter Program. The details of the life cycle of the NBCR geodesically detected using AVISO+ velocity are visually very similar to those of the NBCR detected using MIOST velocity. But there is theoretical reason to expect this. Indeed, while the flow-invariant boundaries of geodesic eddies are of elliptic nature, they follow as limit cycles of a dissipative vector (line) field, which are structurally stable [Arnold, 1973].

## 4 Conclusions

North Brazil Current Rings (NBCRs) do not connect the tropical Atlantic Ocean and the Gulf of Mexico as coherent material vortices despite recent indefensible claims [Huang et al., 2021]. Supported on direct quasi-Lagrangian observations by Frantoni and Richardson [2004], we have provided proof for our rebuttal using *geodesic eddy detection*, a Lagrangian method rooted in geometric nonlinear dynamics [Haller and Beron-Vera, 2013, 2014]. Geodesic vortices detected from satellite altimetry have material (i.e., flow invariant) boundaries that defy stretching in an otherwise typically turbulent ambient fluid. They remain the same independent of whether the observer changes its stand point. Moreover, these boundaries are minimizers of diffusion and stochastic transport transversal to them [Haller et al., 2018]. The main issue with streamline-based, Eulerian eddy detection [Chelton et al., 2011], which forms the basis of the analysis of Huang et al. [2021], lies in its observer-dependent nature, which makes it useless in drawing long-term conclusions about material transport. This issue has been brought up in oceanography many times with unfortunately small reception since at least the work of Beron-Vera et al. [2008].

That some material dragged along by NBCRs that we have been able to classify as material coherent for typically short periods of time can bypass the Lesser Antilles is out of the question. However, once again, this does not happen in an organized, flow-invariant manner. Very intriguingly, that material coherence can be rebuilt in the eastern Caribbean Sea is possible and indeed happens, as it has been shown for the first time recently by Andrade-Canto et al. [2022], in connection with transportation of *Sargassum* and subsequent inundation of coastal areas. The squeezing-through-gaps and subsequent material buildup mechanism proposed by Simmons and Nof [2002] cannot be used to shed light on the problem since NBCRs do not reach the Lesser Antilles as coherent Lagrangian vortices. Why and how material coherence out of incoherent fluid manifests is a fascinating problem that, it seems, will take many years to be elucidated. A seemingly more tractable task is assessing how much fluid initially carried by NBCRs is transported into the Caribbean Sea, which is of interest for varied reasons. Specialized tools to carry out such a task are available [Miron et al., 2021; Drouin et al., 2022; Miron et al., 2022], which will be considered in the future.

The main take-away message from this study is that the oceanographic community, for the reasons exposed above, should exert care when interpreting Eulerian mesoscale eddy data such as those distributed by AVISO+ through the META database.

We close by responding to criticism by two anonymous reviewers, referred to herein as R1 and R2. R1 argued that potential vorticity (PV), as considered in Zhang et al. [2014], should be used in coherent eddy detection instead of geodesic eddy detection as in this paper. R1 advocates the use PV for it being a “dynamical” quantity. We do not ignore the importance of PV for the insight into geophysical fluid dynamics it can provide. However, PV cannot be used to unequivocally frame material coherence because observers that unsteadily rotate and translate relative to one another on the planet will arrive at different conclusions, that is, PV is not objective. This is because the total vorticity itself changes with terrestrial observer’s changes, as it is shown in the online Supporting Information for the case of shallow-water PV on the  $\beta$ -plane. Furthermore, the use of PV in material coherence assessment depends on the so-called PV-barrier argument [Dritschel

and McIntyre, 2008], which is valid for zonally-oriented PV steps and small-amplitude perturbations to them. Obviously, the latter requires material conservation of PV, which in general cannot be expected. By contrast, geodesic eddy detection is objective and is not constrained by PV conservation or any assumption beyond two-dimensionality. R2, in turn, suggested that the Navier–Stokes solutions discussed in the Introduction are irrelevant for geophysical flows. The “o-to-x” behavior illustrated in the middle panels of Fig. 1 is well-documented. Indeed, this paper is one example among many others [Beron-Vera et al., 2013; Haller and Beron-Vera, 2013; Andrade-Canto et al., 2020; Denes et al., 2022]. The “x-to-o” behavior illustrated in the bottom panels of Fig. 1 is less common; Fig. S2 in the Supporting Information provides some evidence of it.

## Acknowledgements

The criticism of two anonymous reviewers has helped us driving the message of our paper more clearly. We thank Daniel Karrasch for the benefit of many useful discussions on geodesic eddy detection implementation and also George Haller for discussions on objectivity. Technical support by A. Dominguez-Guadarrama is acknowledged. FAC was supported by ECOSUR core funding and FJBV by NSF grant OCE2148499.

## Conflict of Interest

The authors declare no conflicts of interest relevant to this study.

## Open Research

The gridded multimission altimeter products <https://www.aviso.altimetry.fr/en/data/data-access.html> including the experimental MIOST product ([https://data.aviso.altimetry.fr/aviso-gateway/data/SLA\\_MIOST\\_alti\\_drifters/](https://data.aviso.altimetry.fr/aviso-gateway/data/SLA_MIOST_alti_drifters/)) were produced by SSALTO/DUACS and distributed by AVISO+, with support from CNES. The META database (<https://data.aviso.altimetry.fr/aviso-gateway/data/META3.1exp.DT/>) was produced by SSALTO/DUACS and distributed by AVISO+, with support from CNES, in collaboration with Oregon State University with support from NASA.

## A AVISO+ vs MIOST

Figure S1 provides a comparison of the life cycle of an NBCR extracted using geodesically detected from AVISO+ velocity data with that of the same NBCR but as geodesically extracted from MIOST velocity data.

## B Evidence of “x-to-o” behavior

Figure S2 provides support to the “x-to-o” behavior illustrated in the bottom panels of Fig 1 based on a geodesic eddy detection from altimetry-derived velocity in the Gulf of Mexico.

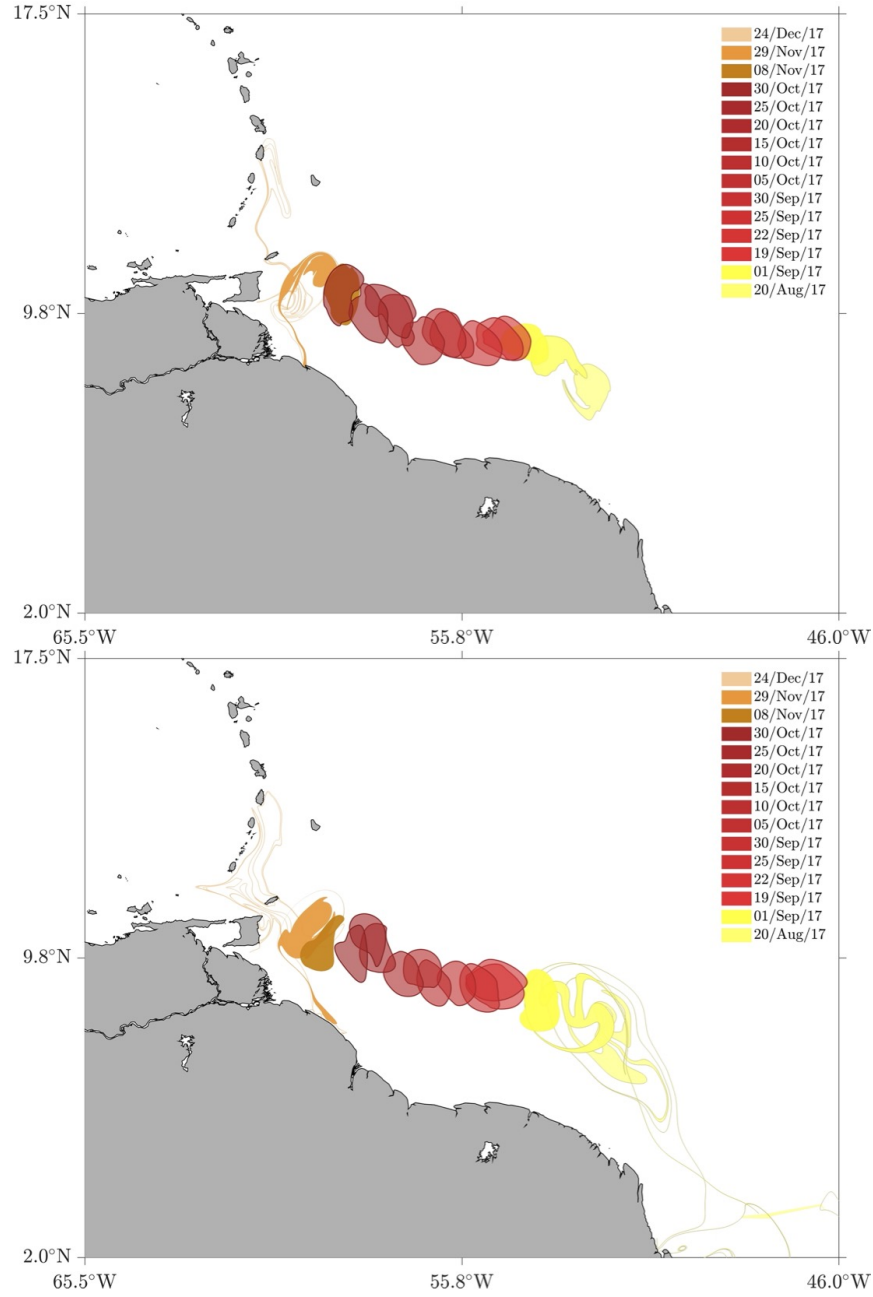


Figure 5: Genesis (yellow), evolution (red), and apocalypse (orange) of a coherent Lagrangian NBCR, geodesically detected from AVISO+ (top) and MIOST (bottom) velocity data.



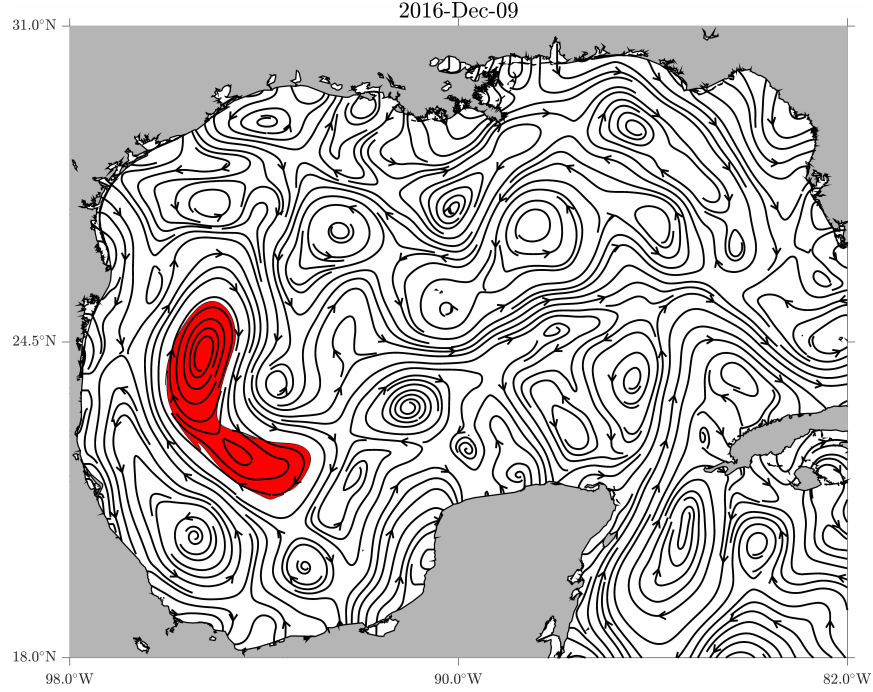


Figure 6: Mesoscale geodesic eddy (red) detected from altimetry-derived velocity in the Gulf of Mexico with instantaneous streamlines of the field overlaid (black curves). Note the instantaneous “x-point” in the center of the coherent material eddy.

## C Observer dependence of the potential vorticity

A scalar field  $s(\mathbf{x}, t)$  on  $\mathbb{R}^2 \times \mathbb{R}$  under the change of observer

$$\mathbf{x} \mapsto \bar{\mathbf{x}} = \begin{pmatrix} \cos \alpha(t) & \sin \alpha(t) \\ -\sin \alpha(t) & \cos \alpha(t) \end{pmatrix} \mathbf{x} + \mathbf{b}(t) \quad (5)$$

transforms as [Truesdell and Noll, 1965]

$$\bar{s}(\bar{\mathbf{x}}, t) = s(\mathbf{x}, t). \quad (6)$$

Now, on the  $\beta$ -plane, the total spin,

$$\Omega_f = \frac{1}{2}(\nabla \mathbf{u}_f - (\nabla \mathbf{u}_f)^\top) = -\frac{1}{2}(\omega + f)J, \quad (7)$$

where  $\omega(\mathbf{x}, t) = \hat{\mathbf{z}} \cdot \nabla \times \mathbf{u}(\mathbf{x}, t)$  is the relative vorticity,  $f(\mathbf{x}) = f_0 + \beta y$  is the Coriolis parameter, and  $J$  represents an  $\frac{1}{2}\pi$ -anticlockwise rotation. This is satisfied by  $\mathbf{u}_f(\mathbf{x}, t) = \mathbf{u}(\mathbf{x}, t) + \mathbf{f}(\mathbf{x})$  for any  $\mathbf{f}$  such that  $\hat{\mathbf{z}} \cdot \nabla \times \mathbf{f} = f$ , which represents the vector potential of the local angular velocity of the planet,  $\frac{1}{2}f\hat{\mathbf{z}}$  [Salmon, 1983]. Under the transformation (5) applied on the  $\beta$ -plane, (7) becomes

$$\bar{\Omega}_f = -\frac{1}{2}(\omega - 2\dot{\alpha} + \varphi)J \quad (8)$$



for some  $\varphi(\mathbf{x}, t)$  such that  $\bar{\nabla}\bar{\mathbf{f}} - (\bar{\nabla}\bar{\mathbf{f}})^\top = -2\varphi J$ . Equation (8) shows how the total vorticity,  $(\omega + f)\hat{\mathbf{z}}$ , changes under a change of  $\beta$ -plane observer (5). Note, in particular, that  $\dot{\alpha}$  is the angular velocity of the observer change. The shallow-water Ertel’s potential vorticity,

$$q = \frac{\omega + f}{h}, \quad (9)$$

where  $h(\mathbf{x}, t)$  is the fluid thickness, then transforms, under (5), as

$$\bar{q} = \frac{\omega - 2\dot{\alpha} + \varphi}{h}, \quad (10)$$

since  $\bar{h} = h$ , as this does not depend on velocity. Thus

$$\bar{q} \neq q. \quad (11)$$

This means that  $q$  changes for terrestrial observers that unsteadily rotate and translate relative to one another, and hence is not objective.

## References

- Adams, D. K. and Flierl, G. R. [2010]. Modeled interactions of mesoscale eddies with the East Pacific Rise: Implications for larval dispersal. *Deep Sea Research Part I: Oceanographic Research Papers* 57, 1163–1176.
- Andrade-Canto, F., Beron-Vera, F. J., Goni, G. J., Karrasch, D., Olascoaga, M. J. and Trinanés, J. [2022]. Carriers of *Sargassum* and mechanism for coastal inundation in the Caribbean Sea. *Phys. Fluids* 34, 016602.
- Andrade-Canto, F., Karrasch, D. and Beron-Vera, F. J. [2020]. Genesis, evolution, and apocalypse of Loop Current rings. *Phys. Fluids* 32, 116603.
- Arnold, V. I. [1973]. *Ordinary Differential Equations*. Massachusetts Institute of Technology.
- Beron-Vera, F. J. and LaCasce, J. H. [2016]. Statistics of simulated and observed pair separations in the gulf of Mexico. *J. Phys. Oceanogr* 46 (7), 2183–2199.
- Beron-Vera, F. J. and Miron, P. [2020]. A minimal Maxey–Riley model for the drift of *Sargassum* rafts. *J. Fluid Mech.* 904, A8.
- Beron-Vera, F. J., Olascoaga, M. J. and Goni, G. J. [2008]. Oceanic mesoscale vortices as revealed by Lagrangian coherent structures. *Geophys. Res. Lett.* 35, L12603.
- Beron-Vera, F. J., Wang, Y., Olascoaga, M. J., Goni, G. J. and Haller, G. [2013]. Objective detection of oceanic eddies and the Agulhas leakage. *J. Phys. Oceanogr.* 43, 1426–1438.
- Chelton, D. B., Schlax, M. G. and Samelson, R. M. [2011]. Global observations of nonlinear mesoscale eddies.
- Denes, M. C., Froyland, G. and Keating, S. R. [2022]. Persistence and material coherence of a mesoscale ocean eddy. *Phys. Rev. Fluids* 7, 034501.
- Didden, N. and Schott, F. [1993]. Eddies in the North Brazil Current retroflection region observed by GEOSAT altimetry. *J. Geophys. Res.* 98, 2,0121–2,0131.
- Dritschel, D. G. and McIntyre, M. E. [2008]. Multiple jets as PV staircases: the Phillips effect and the resilience of eddy-transport barriers. *J. Atmos. Sci.* 65, 855–874.
- Drouin, K. L., Lozier, M. S., Beron-Vera, F. J., Miron, P. and Olascoaga, M. J. [2022]. Surface pathways connecting the South and North Atlantic Oceans. *Geophysical Research Letters* 49 (1), e2021GL096646.
- Edwards, C. A. and Pedlosky, J. [1998]. Dynamics of nonlinear cross-equatorial flow. Part I: Potential vorticity transformation. *Journal of Physical Oceanography* 28, 2382 – 2406.

- Flierl, G. [1981]. Particle motions in large-amplitude wave fields. *Geophys. Astrophys. Fluid Dyn.* 18, 39–74.
- Fratantoni, D. M. and Glickson, D. [2002]. North Brazil Current ring generation and evolution observed with SeaWiFS. *Journal of Physical Oceanography* 32, 1,058–1,074.
- Fratantoni, D. M., Johns, W. E. and Townsend, T. L. [1995]. Rings of the North Brazil Current: Their structure and behavior inferred from observations and a numerical simulation. *Journal of Geophysical Research* 100, 10633.
- Fratantoni, D. M. and Richardson, P. L. [2004]. The evolution and demise of North Brazil Current rings. *J. Phys. Oceanogr.* 36, 1241–1264.
- Garraffo, Z., Johns, W. E., Chassignet, E. and Goni, G. J. [2003]. North Brazil Current rings and transport of southern waters in a high resolution numerical simulation of the North Atlantic. In *Interhemispheric Water Exchange in the Atlantic Ocean* (ed. P. Malanotte-Rizzoli and G. J. Goni), pp. 375–410. Elsevier Oceanography Series 68, Elsevier Science.
- Goni, G. and Johns, W. [2001]. Census of warm rings and eddies in the North Brazil Current retroflection region from 1992 through 1998 using TOPEX/Poseidon altimeter data. *Geophys. Res. Lett.* 28, 1–4.
- Goni, G. J. and Johns, W. [2003]. Synoptic study of North Brazil Current rings from altimetry, in interhemispheric water exchange in the Atlantic Ocean. In *Interhemispheric Water Exchange in the Atlantic Ocean* (ed. G. J. Goni and P. Malanotte-Rizzoli), pp. 335–356. Elsevier Oceanography Series 68, Elsevier Science.
- Haller, G. [2005]. An objective definition of a vortex. *J. Fluid Mech.* 525, 1–26.
- Haller, G. [2015]. Lagrangian coherent structures. *Ann. Rev. Fluid Mech.* 47, 137–162.
- Haller, G. and Beron-Vera, F. J. [2012]. Geodesic theory of transport barriers in two-dimensional flows. *Physica D* 241, 1680–1702.
- Haller, G. and Beron-Vera, F. J. [2013]. Coherent Lagrangian vortices: The black holes of turbulence. *J. Fluid Mech.* 731, R4.
- Haller, G. and Beron-Vera, F. J. [2014]. Addendum to ‘Coherent Lagrangian vortices: The black holes of turbulence’. *J. Fluid Mech.* 755, R3.
- Haller, G., Karrasch, D. and Kogelbauer, F. [2018]. Material barriers to diffusive and stochastic transport. *Proceedings of the National Academy of Sciences* 115, 9074–9079.
- Huang, M., Liang, X., Zhu, Y., Liu, Y. and Weisberg, R. H. [2021]. Eddies connect the tropical Atlantic Ocean and the Gulf of Mexico. *Geophysical Research Letters* 48, e2020GL091277.
- Jochum, M. and Malanotte-Rizzoli, P. [2003]. On the generation of North Brazil Current rings. *Journal of Marine Research* 61, 147–173.
- Johns, E. M., Muhling, B. A., Perez, R. C., Müller-Karger, F. E., Melo, N., Smith, R. H., Lamkin, J. T., Gerard, T. L. and Malca, E. [2014]. Amazon river water in the northeastern caribbean sea and its effect on larval reef fish assemblages during april 2009. *Fisheries Oceanography* 23, 472–494.
- Johns, W. E., Lee, T. N., Schott, F. A., Zantopp, R. J. and Evans, R. H. [1990]. The North Brazil Current retroflection: Seasonal structure and eddy variability. *Journal of Geophysical Research* 95, 22103.
- Johns, W. E., Zantopp, R. and Goni, G. J. [2003]. Cross-gyre transport by North Brazil Current rings. In *Interhemispheric Water Exchange in the Atlantic Ocean* (ed. P. Malanotte-Rizzoli and G. J. Goni), pp. 411–442. Elsevier Oceanography Series 68, Elsevier Science.
- Karrasch, D., Huhn, F. and Haller, G. [2014]. Automated detection of coherent Lagrangian vortices in two-dimensional unsteady flows. *Proc. Royal Soc. A* 471, 20140639.
- Karrasch, D. and Schilling, N. [2020]. Fast and robust computation of coherent Lagrangian vortices on very large two-dimensional domains. *The SMAI Journal of Computational Mathematics* 6, 101–124.
- Lugt, H. J. [1979]. The dilemma of defining a vortex. In *Recent Developments in Theoretical and Experimental Fluid Mechanics* (ed. U. Muller, K. G. Riesner and B. Schmidt), pp. 309–321.

- Springer-Verlag.
- Miron, P., Beron-Vera, F. J., Helfmann, L. and Koltai, P. [2021]. Transition paths of marine debris and the stability of the garbage patches. *Chaos* 31, 033101.
- Miron, P., Beron-Vera, F. J. and Olascoaga, M. J. [2022]. Transition paths of North Atlantic Deep Water. *J. Atmos. Oce. Tech.* 39, 959–971.
- Pedergnana, T., Oettinger, D., P. Langlois, G. and Haller, G. [2020]. Explicit unsteady navier–stokes solutions and their analysis via local vortex criteria. *Physics of Fluids* 32 (4), 046603.
- Pegliasco, C., Delepouille, A., Mason, E., Morrow, R., Faugère, Y. and Dibarboure, G. [2022]. META3.1exp: a new global mesoscale eddy trajectory atlas derived from altimetry. *Earth System Science Data* 14, 1087–1107.
- Poje, A. C., Özgökmen, T. M., Bogucki, D. J. and Kirwan, A. D. [2017]. Evidence of a forward energy cascade and kolmogorov self-similarity in submesoscale ocean surface drifter observations. *Physics of Fluids* 29, 020701.
- Rio, M.-H., Guinehut, S. and Gilles, L. [2011]. New CNES–CLS09 global mean dynamic topography computed from the combination of GRACE data, altimetry, and in situ measurements. *Journal of Geophysical Research* 116, C07018.
- Robinson, A. R., ed. [1983]. *Eddies in Marine Science*. Springer-Verlag.
- Salmon, R. [1983]. Practical use of Hamilton’s principle. *J. Fluid Mech.* 132, 431–444.
- Schlag, M. G. and Chelton, D. B. [2016]. The “Growing Method” of eddy identification and tracking in two and three dimensions. Corvallis, Oregon: College of Earth, Ocean and Atmospheric Sciences, Oregon State University.
- Simmons, H. and Nof, D. [2002]. The squeezing of eddies through gaps. *J. Phys. Oceanogr.* 32, 314–335.
- Truesdell, C. and Noll, W. [1965]. *The Non-Linear Field Theories of Mechanics*. New York: Springer.
- Wilson, D. W., Johns, W. E. and Garzoli, S. L. [2002]. Velocity structure of the North Brazil Current rings. *Geophys. Res. Lett.* 29, 314–335.
- Zhang, Z., Wang, W. and Qiu, B. [2014]. Oceanic mass transport by mesoscale eddies. *Science* 345, 322–324.
- Zharkov, V. and Nof, D. [2010]. Why does the North Brazil Current regularly shed rings but the Brazil Current does not? *Journal of Physical Oceanography* 40, 354 – 367.